NANO LETTERS

2004
Vol. 4, No. 1
55−59

Room Temperature Negative Differential Resistance through Individual Organic Molecules on Silicon Surfaces

Nathan P. Guisinger, Mark E. Greene, Rajiv Basu, Andrew S. Baluch, and Mark C. Hersam*

Department of Materials Science and Engineering, Northwestern University, Evanston, Illinois 60208

Received October 2, 2003

ABSTRACT

Room temperature negative differential resistance (NDR) has been measured through individual organic molecules on degenerately doped Si(100) surfaces using ultrahigh vacuum scanning tunneling microscopy (STM). For styrene molecules on n-type Si(100), NDR is observed only for negative sample bias because positive sample bias leads to electron stimulated desorption. By replacing styrene with a saturated organic molecule (2,2,6,6-tetramethyl-1-piperidinyloxy), electron stimulated desorption is not observed at either bias polarity. In this case, NDR is observed only for negative sample bias on n-type Si(100) and for positive sample bias on p-type Si(100). This unique behavior is consistent with a resonant tunneling mechanism via molecular orbitals and opens new possibilities for silicon-based molecular electronic devices and chemical identification with STM at the single-molecule level.

Since Aviram and Ratner's seminal 1974 paper,[1] the promise of molecular electronic devices has united chemists, physicists, and engineers in the interdisciplinary pursuit of understanding and utilizing charge transport at the single-molecule level. The simplest molecular electronic component—one molecule between two metal electrodes—has recently been demonstrated by several groups,[2] leading to diverse charge transport behavior including gaps in conduction,[3] coulomb blockade,[4] current rectification,[5] bistable switching,[6] conformational switching,[7] stochastic switching,[8] negative differential resistance (NDR),[9] and Kondo resonance.[10,11] Although the choice of molecule plays a critical role in the operation of metal−molecule−metal junctions, the interface between the molecule and the electrodes has come under increasing scrutiny due to limited agreement between experimental and theoretical analyses.[12] The apparent importance of the contacts in molecular electronic devices suggests that alternative electrode materials may lead to unique charge transport phenomena. For example, recent results show that self-assembled organic monolayers on silicon lead to current rectification.[13]

Here we report room temperature charge transport measurements performed on individual organic molecules mounted on degenerately doped Si(100) surfaces using ultrahigh vacuum (UHV) scanning tunneling microscopy (STM). Under appropriate biasing and doping conditions, NDR is observed through individual molecules at room temperature. In previous STM studies, NDR has been observed for thiol molecules on gold surfaces,[14,15] boron dopant atoms on Si(111) surfaces,[16,17] and boron-doped polycrystalline diamond films.[18] In each of these cases, NDR has been attributed to resonant tunneling between localized states on the STM tip and the surface. Because the detailed electronic structure of the tip varies during an experiment, NDR in these cases occurs at a variety of bias magnitudes and both bias polarities.[19] However, in our measurements, NDR always occurs at a particular bias polarity based on the doping of the Si(100) substrate. Furthermore, multiple NDR events are observed in a given current−voltage curve. These observations are consistent with a resonant tunneling mechanism between the bulk silicon band structure and the discrete orbitals of the adsorbed molecule. Through appropriate choice of molecule and substrate doping, the details of the charge transport and the stability of the semiconductor−molecule junction can be tuned. Technologically, these results suggest that a new class of molecular electronic devices may be possible on the Si(100) surface, thus opening opportunities for hybrid molecular electronic and conventional microelectronic circuitry. From a more fundamental perspective, analysis of the STM spectroscopic data may allow for chemical identification and quantitative assignment of surface-mounted molecular orbital energy levels at the single-molecule level.

All experiments were performed in a custom-built room-temperature UHV STM, which maintains a base pressure

* Corresponding author. E-mail: m-hersam@northwestern.edu.

10.1021/nl0348589 CCC: $27.50
Published on Web 11/01/2003

less than 5×10^{-11} Torr. The scanner is a Lyding design[20] and is controlled by digital feedback electronics. The UHV system consists of a sample preparation chamber and a chamber housing the STM scanner, both of which have separate ion pumps and are isolated by a gate valve to minimize cross contamination. An external gas manifold houses the molecular species, which are introduced into the STM chamber via one of two independent leak valves. The molecular species themselves are loaded into custom designed glass vials that have been thoroughly cleaned, degreased, and heated to promote removal of moisture and unwanted residual organics. All handling of molecular species and vial loading is conducted in a controlled atmosphere glovebox (Vacuum Atmospheres Nexus model) that maintains water and oxygen levels of less than 1 ppm. After mounting to the UHV chamber gas manifold, the loaded vials undergo a series of freeze−pump−thaw cycles with liquid nitrogen.

The experiments were performed on Si(100) substrates (Virginia Semiconductor), which were degenerately n-type or p-type doped with arsenic or boron, respectively, with a resistivity of <0.005 Ω-cm. All samples were degreased with acetone and isopropyl alcohol ex situ. Immediately following introduction to UHV, the samples were degassed at 600 °C for >12 h. To prepare an atomically pristine Si(100) 2×1 reconstructed surface, the degassed sample was flashed in the UHV preparation chamber at a temperature of 1250 °C for 30 s. The prepared sample was characterized with the STM prior to molecular dosing to ensure atomic-level cleanliness and the 2×1 reconstruction. All imaging was performed in constant current mode with a tunneling current of 0.1 nA and a sample bias of −2 V relative to a grounded tip. The STM tip was fabricated via electrochemical etching with W or PtIr wire. The experimental results show no measurable dependence on the tip material.

Following surface verification, the sample is moved out of tunneling range on the STM, and dosing is initiated. In this paper, two different commercially available molecules were studied: styrene and 2,2,6,6-tetramethyl-1-piperidinyloxy (TEMPO). For both molecules, a uniform submonolayer coverage was achieved at an optimal dose of 0.006 L (1×10^{-10} Torr for 1 min). After dosing, the sample was returned to tunneling range and imaged with the STM. For the given dosing conditions, the molecular species were easily identified as protrusions in the topographic images. STM spectroscopy was implemented at several locations, both on the molecular adsorbates and on the clean Si(100) surface. Concurrent topographic scanning ensured an accurate assessment of the spatial position of each STM spectrum. During STM spectroscopy, the tip position is held constant at the height established by the constant current feedback conditions of −2 V and 0.1 nA. The sample voltage is then swept from −5 V to +5 V, while recording the tunneling current. The gain of the current preamplifier was set at a value of 10^9, which limits the magnitude of the measured current range to 2.75 nA. Current values exceeding this threshold result in saturation of the detector, as observed in some of the current−voltage measurements near the upper and lower bounds of the sweep voltage.

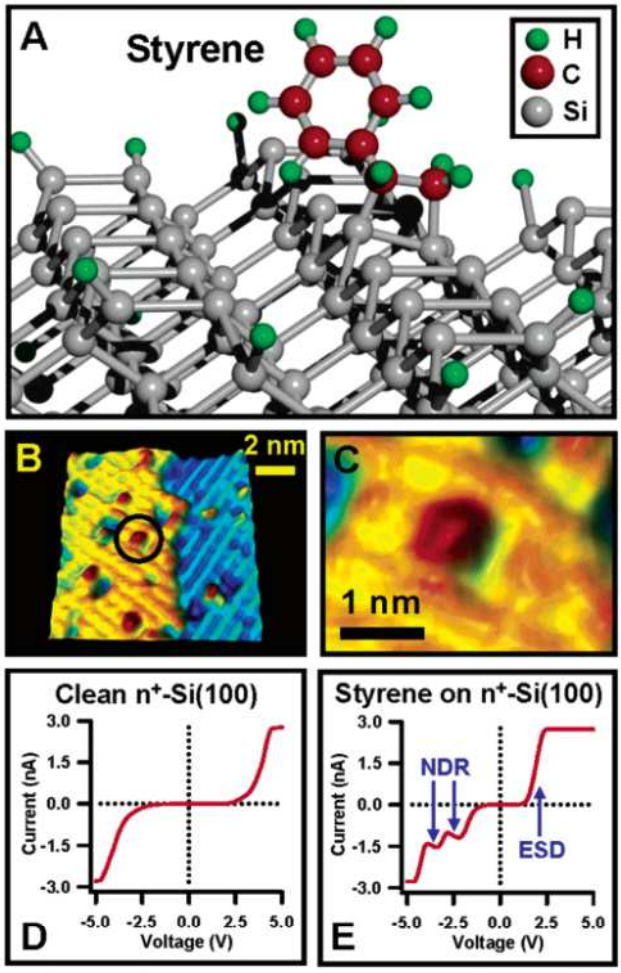

Figure 1. Styrene on the Si(100)-2×1 surface. (A) Schematic representation of an individual styrene molecule bound to a truncated Si(100) surface following molecular mechanics optimization. (B) STM topography image of isolated styrene molecules bound to the degenerately n-type Si(100)-2×1 surface. The black circle identifies a single styrene molecule chosen for STM spectroscopy. (C) STM image of the circled styrene molecule prior to current−voltage characterization. (D) Current−voltage curve measured on the clean Si(100)-2×1 surface within the vicinity of the isolated styrene molecules. (E) Current−voltage curve measured over the isolated styrene molecule. Negative sample bias reveals two distinct NDR events, whereas ESD is detected at positive sample bias.

Initial experiments were performed for styrene molecules on degenerately n-type Si(100). Figure 1A contains a molecular mechanics calculation for the expected geometry of styrene bound to two dangling bonds on the clean Si(100) surface.[21] The calculation is consistent with previous reports.[22] Figure 1B is an overview STM image of the Si(100) surface following styrene deposition, while Figure 1C is focused on an individual styrene molecule. In this intramolecular resolution image, the portion of the molecule bound to the silicon dimer appears as a depression, whereas the aromatic ring appears as a protrusion. The apparent depression is likely caused by the reduced density of electronic states for the reacted silicon dimer compared to

the dangling bonds on the remainder of the silicon surface. After identifying the styrene molecules on the surface, STM spectroscopy was performed at several locations both over the surface adsorbates and on the clean Si(100) surface. Figure 1D shows a typical current−voltage curve taken on the clean Si(100) surface. The curve is relatively featureless and is consistent with previous reports.[23] No apparent topographical changes are observed on the bare Si(100) surface following STM spectroscopy. Figure 1E contains a current−voltage curve taken directly over a styrene molecule. Unlike Figure 1D, two clear NDR events are detected at negative sample bias. At positive sample bias, the current rapidly increases and saturates the detector. Following this measurement, the styrene molecule is no longer observed on the surface in STM topography images. Consequently, we attribute the abrupt increase in current at positive sample bias to electron stimulated desorption (ESD) of the styrene molecule. It should be noted that previous studies have found organic molecules containing π bonds to be especially susceptible to ESD.[22,24,25]

To minimize the likelihood of ESD, a saturated hydrocarbon was chosen for subsequent studies of NDR in molecule−semiconductor−metal junctions. In particular, the oxygen free radical, TEMPO, reacts with a single dangling bond on the Si(100) to form a covalent Si−O bond as shown in Figure 2A.[21] The single binding point of TEMPO to the Si(100) surface minimizes possible binding conformations and lends itself to atomic resolution patterning via feedback controlled lithography.[26] Figures 2B and 2C contain STM images of an n-type Si(100) surface following deposition of TEMPO. The TEMPO molecule appears as a clear protrusion that is slightly offset from the center of the silicon dimer. Figure 2D shows STM spectroscopy results for an individual TEMPO molecule on an n-type Si(100) surface. As was observed for styrene, the TEMPO current−voltage curve contains multiple NDR events at negative sample bias. However, unlike styrene, the TEMPO molecule does not undergo ESD, and current data is detected at positive sample bias. Of particular interest is a shoulder in the current−voltage curve at high positive sample bias. Figure 2E contains STM spectroscopy data for an individual TEMPO molecule on a p-type Si(100) surface. The current−voltage curve contains the same qualitative features as Figure 2D except at the opposite bias polarity. Specifically, two NDR events are detected at positive sample bias, and a discontinuity is observed in the current−voltage curve at negative sample bias. The behavior observed in each of the current−voltage curves was verified on multiple samples with multiple tips. Although the exact bias for NDR or shoulders varied from experiment to experiment, these events always occurred at the same bias polarity for a given doping type.

The observed current−voltage behavior is consistent with a resonant tunneling mechanism recently proposed by Datta et al.[27] Figure 3 schematically illustrates energy band diagrams that summarize the charge transport mechanism. Figures 3A and 3D show equilibrium band diagrams for n-type and p-type silicon, respectively. Although band bending is shown at the silicon surface to maintain consistency with the model of Datta et al., the degree of band bending plays a relatively minor role since NDR is determined by the bulk silicon band-edges.[27] The location of the Fermi level, E_F, with respect to the lowest unoccupied molecular orbital (LUMO) and the highest occupied molecular orbital (HOMO) is adjusted for consistency with the measured data.[28] Under an applied bias, V, the electrostatic potential on the molecule is assumed to be $\sim V/2$, in agreement with previous calculations.[29] Figure 3B considers the situation where a negative bias is applied to the n-type sample with respect to the grounded metal tip. At a critical applied bias, the electrochemical potential of the sample, μ_1, aligns with the LUMO, leading to resonant tunneling and a peak in the conduction. At a bias slightly higher than this critical value, the narrow band of conduction electrons moves off resonance. Due to the presence of the conduction band

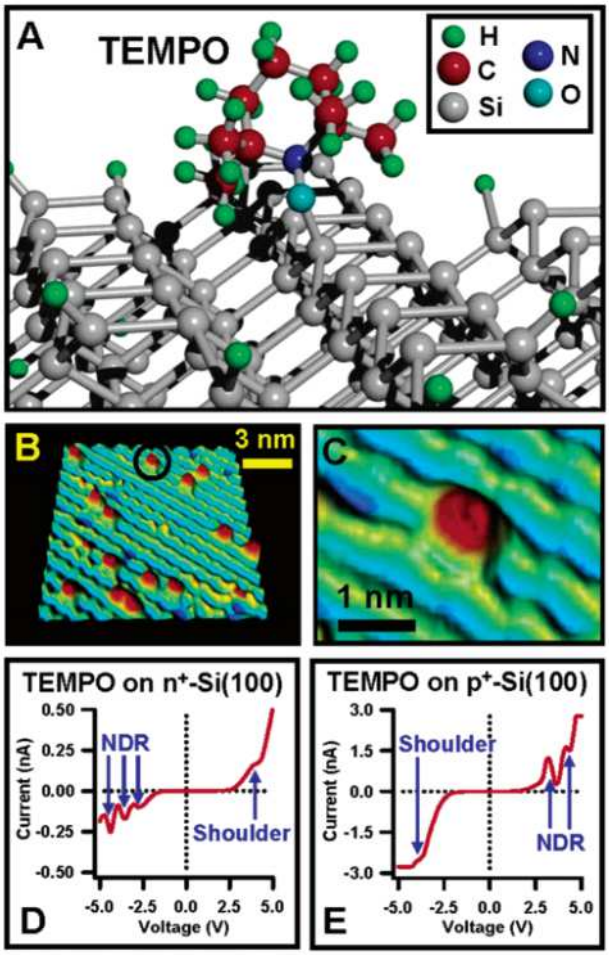

Figure 2. TEMPO on the Si(100)-2 × 1 surface. (A) Molecular mechanics optimized structure of an individual TEMPO molecule on a truncated Si(100)-2 × 1 surface. (B) STM topography image of isolated TEMPO molecules on a degenerately n-type Si(100)-2 × 1 surface. (C) STM image of the isolated TEMPO molecule that is circled in part (B). (D) Current−voltage plot of an isolated TEMPO molecule bound to n-type Si(100). At negative sample bias, three distinct NDR events are observed, while a shoulder is observed at positive sample bias. (E) Current−voltage plot of an isolated TEMPO molecule bound to p-type Si(100). At negative sample bias, a discontinuity is observed, whereas two NDR events are detected at positive sample bias.

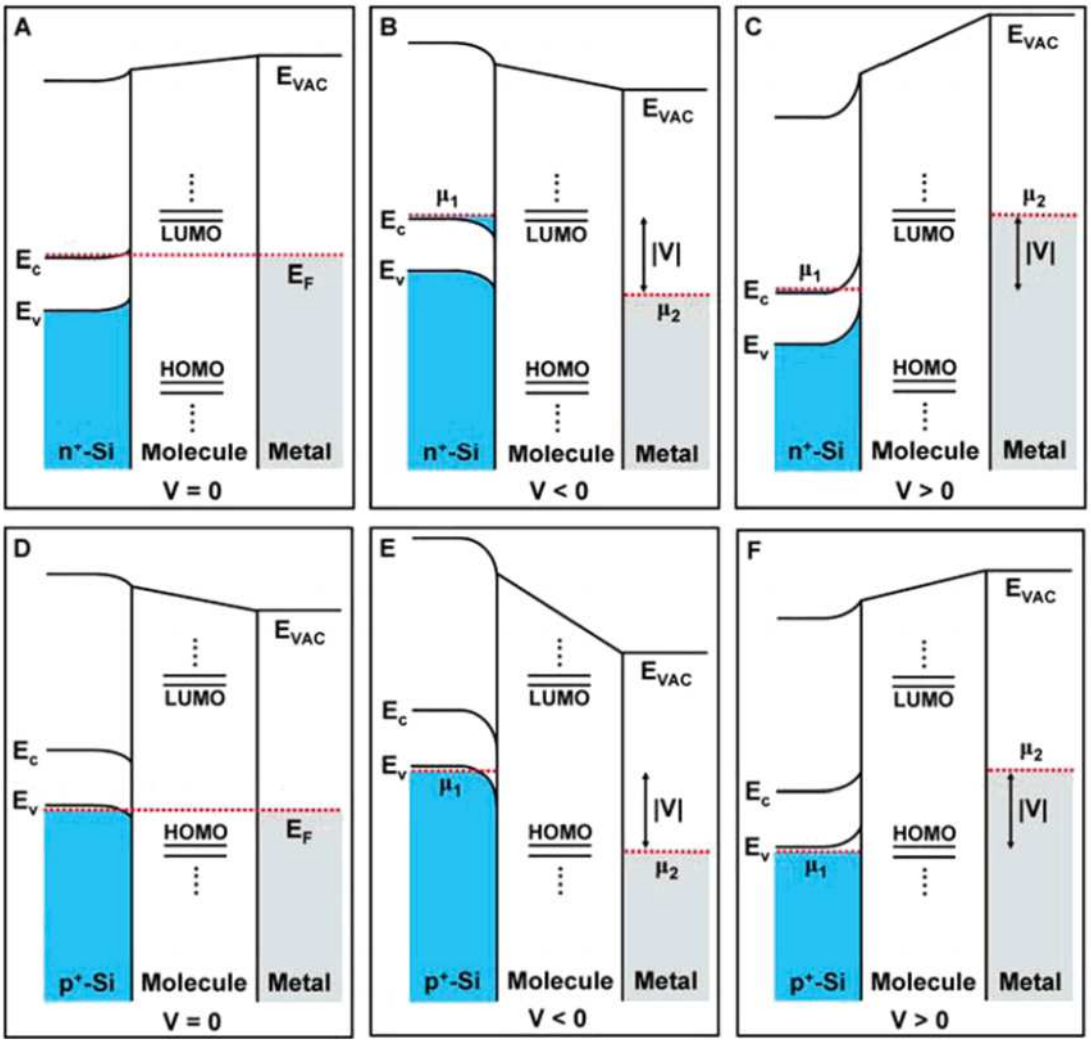

Figure 3. Energy band diagrams. (A−C) Energy band diagrams depicting the semiconductor−molecule−metal junction for degenerately doped n-type Si(100) at (A) equilibrium, (B) negative sample bias, and (C) positive sample bias. (D−F) Energy band diagrams depicting the semiconductor−molecule−metal junction for degenerately doped p-type Si(100) at (D) equilibrium, (E) negative sample bias, and (F) positive sample bias.

edge, E_C, and the onset of the silicon band gap, the conduction at this bias level will decrease, leading to NDR. At even higher negative sample biases, μ_1 will move on and subsequently off resonance with higher unoccupied molecular orbitals. In agreement with the experimental data, this band diagram predicts multiple NDR events at negative sample bias for molecules adsorbed to degenerately n-type doped silicon.

Figure 3C depicts the situation for the opposite polarity on n-type silicon. In this case, the electrochemical potential of the metal tip, μ_2, will align with the LUMO. This alignment implies the opening of another conduction pathway that will lead to a discontinuous increase in the current. However, unlike the semiconducting substrate, the metal tip does not possess a band gap. Consequently, further bias increases do not lead to NDR, thus explaining the presence of the shoulder at positive sample bias in Figure 2D. Figures 3E and 3F consider p-type silicon samples under negative and positive sample bias, respectively. This situation is analogous to n-type silicon except that the electrochemical potentials of the sample and the tip move into alignment with the HOMO and lower occupied molecular orbitals of the adsorbed molecule. In addition, the valence band edge, E_V, of the p-type substrate plays the analogous role of E_C in the n-type case. These differences imply that the prominent features in the current−voltage curves for p-type substrates have the opposite polarity of n-type substrates. In other words, multiple NDR events are expected at positive sample bias and a shoulder is expected at negative sample bias for p-type substrates. The measured data in Figure 2E is consistent with this explanation. Overall, the relatively simple physical description schematically depicted by the energy band diagrams of Figure 3 qualitatively reproduces all of the observed behavior.

Although the polarity of the observed NDR is highly reproducible, the exact value of the NDR bias varies by as much as 1 V from experiment to experiment. Since the details of the electrostatic potential distribution across the molecule are highly sensitive to the tip−sample spacing,[27] the variability in the NDR bias value may be attributed to subtle

variations in tip−sample spacing. Other variables that may influence the NDR bias value include the presence of defects (e.g., buckled dimers, missing dimers, other molecules, step edges, etc.) in close proximity to the adsorbed molecule. Consistent with this latter explanation, our measurements on disordered molecular monolayers show wide variability and attenuation of the NDR effect compared to isolated molecules.

In summary, we have measured room temperature NDR through individual organic molecules on degenerately doped Si(100) surfaces. The observed behavior is consistent with a resonant tunneling mechanism between the narrow band of free charge carriers in the semiconductor substrate and the molecular orbitals of the surface adsorbate. In contrast to molecular electronic studies on metal substrates that have been dominated by organic molecules with π bonds, saturated hydrocarbons are among the best candidates for robust molecular electronic devices on silicon due to their resistance to ESD. From a technological perspective, the achievement of room temperature NDR on silicon opens up the possibility of hybrid molecular and microelectronic circuits that can efficiently implement logic operations[30] and refresh random access memory cells.[31] Furthermore, quantitative assignment of NDR to molecular orbital levels may allow for chemical identification of individual molecules on silicon surfaces with STM.

Acknowledgment. We thank S. Datta (Purdue University) for suggesting and predicting NDR measurements on individual molecules on silicon, J. Michl (University of Colorado) for proposing the TEMPO chemistry, and E. T. Foley (Northwestern University) for helpful discussions. This work was supported by an Arnold and Mabel Beckman Young Investigator Award, the NASA Institute for Nanoelectronics and Computing under Award Number NCC 2-3163, the Nanoscale Science and Engineering Initiative of the National Science Foundation under NSF Award Numbers EEC-0118025 and DMR-0134706, and the Defense University Research Initiative in Nanotechnology of the United States Army Research Office under Grant Number DAAD 19-01-1-0521.

References

(1) Aviram, A.; Ratner, M. A. *Chem. Phys. Lett.* **1974**, *29*, 277−283.
(2) Service, R. F. *Science* **2001**, *294*, 2442−2443.
(3) Reed, M. A.; Zhou, C.; Muller, J.; Burgin, T. P.; Tour, J. M. *Science* **1997**, *278*, 252−254.
(4) Andres, R. P.; Bein, T.; Dorogi, M.; Feng, S.; Henderson, J. I.; Kubiak, C. P.; Mahoney, W.; Osifchin, R. G.; Reifenberger, R. *Science* **1996**, *272*, 1323−1325.
(5) Metzger, R. M. *J. Mater. Chem.* **2000**, *10*, 55−62.
(6) Collier, C. P.; Mattersteig, G.; Young, E. W.; Luo, Y.; Beverly, K.; Sampaio, J.; Raymo, F. M.; Stoddart, J. F.; Heath, J. R. *Science* **2000**, *289*, 1172−1175.
(7) Donhauser, Z. J.; Mantooth, B. A.; Kelley, K. F.; Bumm, L. A.; Monnell, J. D.; Stapleton, J. J.; Price, D. W., Jr.; Rawlett, A. M.; Allara, D. L.; Tour, J. M.; Weiss, P. S. *Science* **2001**, *292*, 2303−2307.
(8) Ramachandran, G. K.; Hopson, T. J.; Rawlett, A. M.; Nagahara, L. A.; Primak, A.; Lindsay, S. M. *Science* **2003**, *300*, 1413−1416.
(9) Chen, J.; Reed, M. A.; Rawlett, A. M.; Tour, J. M. *Science* **1999**, *286*, 1550−1552.
(10) Park, J.; Pasupathy, A. N.; Goldsmith, J. I.; Chang, C.; Yaish, Y.; Petta, J. R.; Rinkoski, M.; Sethna, J. P.; Abruña, H. D.; McEuen, P. L.; Ralph, D. C. *Nature* **2002**, *417*, 722−725.
(11) Liang, W.; Shores, M. P.; Bockrath, M.; Long, J. R.; Park, H. *Nature* **2002**, *417*, 725−729.
(12) Nitzan, A.; Ratner, M. A. *Science* **2003**, *300*, 1384−1389.
(13) Lenfant, S.; Krzeminski, C.; Delerue, C.; Allan, G.; Vuillaume, D. *Nano Lett.* **2003**, *3*, 741−746.
(14) Xue, Y.; Datta, S.; Hong, S.; Reifenberger, R.; Henderson, J. I.; Kubiak, C. P. *Phys. Rev. B* **1999**, *59*, R7852−R7855.
(15) Fan, F. F.; Yang, J.; Cai, L.; Price, D. W., Jr.; Dirk, S. M.; Kosynkin, D. V.; Yao, Y.; Rawlett, A. M.; Tour, J. M.; Bard, A. J. *J. Am. Chem. Soc.* **2002**, *124*, 5550−5560.
(16) Lyo, I.-W.; Avouris, Ph. *Science* **1989**, *245*, 1369−1371.
(17) Bedrossian, P.; Chen, D. M.; Mortensen, K.; Golovchenko, J. A. *Nature* **1989**, *342*, 258−260.
(18) Ma, D. D. D.; Wang, Y. G.; Lu, L.; Lee, C. S.; Lee, S. T. *Appl. Phys. Lett.* **2002**, *80*, 1231−1233.
(19) Avouris, Ph.; Lyo, I.-W.; Bozso, F.; Kaxiras, E. *J. Vac. Sci. Technol. A* **1990**, *8*, 3405−3411.
(20) Lyding, J. W.; Skala, S.; Hubacek, J. S.; Brockenbrough, R.; Gammie, G. *Rev. Sci. Instrum.* **1988**, *59*, 1897−1902.
(21) All calculations were carried out using HyperChem Release 7 (Hypercube, Inc., Gainesville, FL). The geometries of the individual TEMPO and styrene molecules were optimized at the level of B3LYP density functional theory using the polarized 6-31G* basis via the eigenvector following algorithm. The 4 × 4 × 1 Si(100) crystal was optimized using the MM+ molecular mechanics force field using the Polak−Ribiere conjugate-gradient algorithm. The 2 × 1 reconstruction was forced by allowing only the top layer of atoms to optimize their spacings after the original slab optimization. The resulting dimer spacing after MM optimization was 3.82 Å compared to a measured value of 3.85 Å. Hydrogen atoms were added to the periphery of the silicon slab to quench unpaired electrons. Styrene was bound to the most central dimer, while TEMPO was bound to the most central silicon atom. In both cases, the organic molecule and the silicon atoms to which each was bonded were allowed to relax to an energetic minimum via the MM+ force field and the PR algorithm.
(22) Patitsas, S. N.; Lopinski, G. P.; Hul'ko, O.; Moffatt, D. J.; Wolkow, R. A. *Surf. Sci.* **2000**, *457*, L425−L431.
(23) Hamers, R. J.; Avouris, Ph.; Bozso, F. *Phys. Rev. Lett.* **1987**, *59*, 2071−2074.
(24) Alavi, S.; Rousseau, R.; Patitsas, S. N.; Lopinski, G. P.; Wolkow, R. A.; Seideman, T. *Phys. Rev. Lett.* **2000**, *85*, 5372−5375.
(25) Kruse, P.; Wolkow, R. A. *Appl. Phys. Lett.* **2002**, *81*, 4422−4424.
(26) Hersam, M. C.; Guisinger, N. P.; Lyding, J. W. *Nanotechnology* **2000**, *11*, 70−76.
(27) Rakshit, T.; Liang, G.-C.; Ghosh, A. W.; Datta, S. **2003**, cond-mat/0305695.
(28) The exact location of the molecular orbital energy level with respect to the substrate Fermi level will be a function of the degree of charge transfer between the molecule and the substrate. Consequently, the difference in the molecular orbital spacing with respect to the Fermi level in Figures 3A and 3D can be justified by assuming that the charge transfer depends on the substrate doping type.
(29) Datta, S.; Tian, W.; Hong, S.; Reifenberger, R.; Henderson, J. I.; Kubiak, C. P. *Phys. Rev. Lett.* **1997**, *79*, 2530−2533.
(30) Mathews, R. H.; Sage, J. P.; Sollner, T. C. L. G.; Calawa, S. D.; Chen, C. L.; Mahoney, L. J.; Maki, P. A.; Molvar, K. M. *Proc. IEEE* **1999**, *87*, 596−605.
(31) van der Wagt, J. P. A.; Seabaugh, A. C.; Beam, E. A. *IEEE Electron Device Lett.* **1998**, *19*, 7−9.

NL0348589